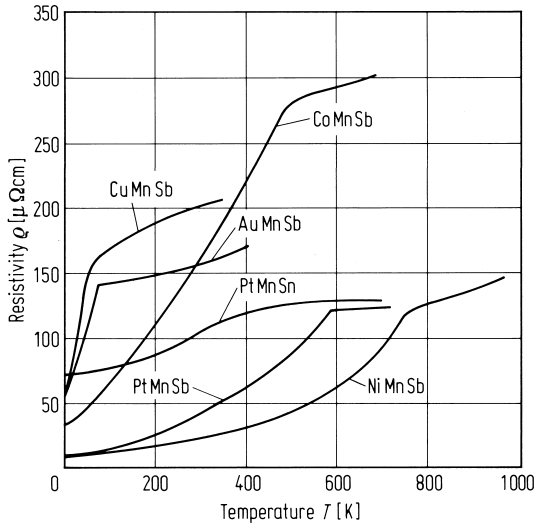

Fig. 291. Electrical resistivity ρ as a function of temperature for several $C1_b$ compounds [87O3].

over the temperature range 4…800 K. At low temperatures the resistivity of ferromagnets usually has a term proportional to T^2, due to spinflip scattering. However, this spinflip scattering is not possible in a half metallic-ferromagnet, because there are no states with the opposite spin orientation at the Fermi level at low temperatures. Neither NiMnSb nor PtMnSb exhibits a T^2 dependence in the low temperature resistivity.

1.5.5.6.2 Galvanomagnetic properties

X_2YZ X = 3d, Y = 3d

X = 8A: Ni
Y = 7A: Mn
Z = 3B: In; 4B: Sn; 5B: Sb

Ni_2MnZ

The galvanomagnetic properties have been investigated in order to quantify the effects of changing the electron concentration. Systematic effects are observed as the Fermi level is shifted, which have been interpreted using a delocalised description of the electron transport effects.

The transverse magneto-resistance of the three compounds containing In, Sn or Sb is similar to and typical for a ferromagnet. The field dependence of the Hall resistivity $\rho_{21}(B)$ has two parts: one saturating below ≈ 1 T and another that varies linearly with field. The former is the anomalous Hall effect (AHE) which is prominent in ferromagnets, exhibiting a bend in its field dependence. The anomalous Hall angle used to distinguish the microscopic scattering mechanism at an M site is defined by:

$$\theta_E = \theta_\hbar(T) = \left[\frac{\Delta\rho_{21}(T)}{\rho_0(T)}\right]\left(1/M_s^1\right) \tag{65}$$

where

$$M_s^1(T) = M_s(T)/M_s(4.2\text{K}) \tag{66}$$

The ordinary Hall coefficient R_0 is estimated from the gradient of $\rho_{21}(B)$ above saturation and at 4.2 K where complications from phonon scattering are minimised.

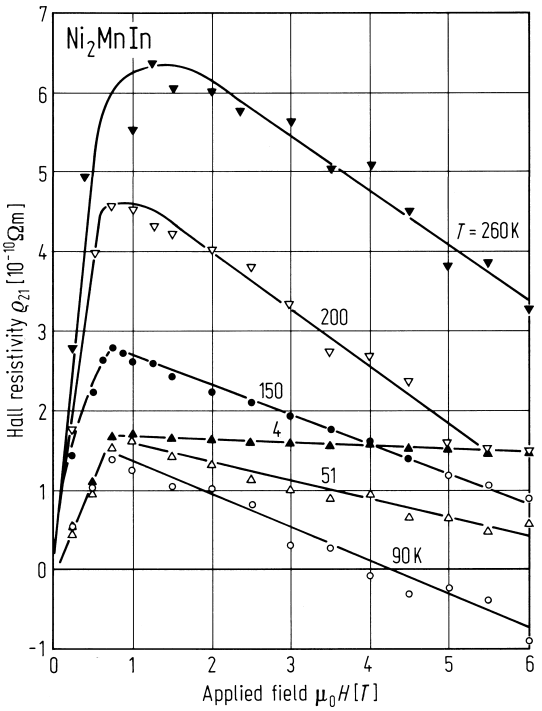

Fig. 292. Field dependence of the Hall resistivity of Ni_2MnIn at different temperatures. *H* is the applied field and the abscissa unit corresponds to a flux density of 1T [86H2].

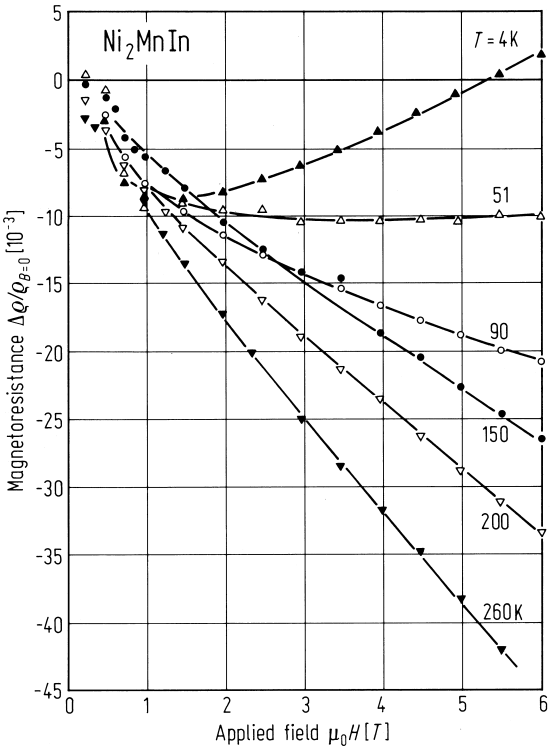

Fig. 293. Transverse magnetoresistance of Ni_2MnIn at different temperatures [86H2].

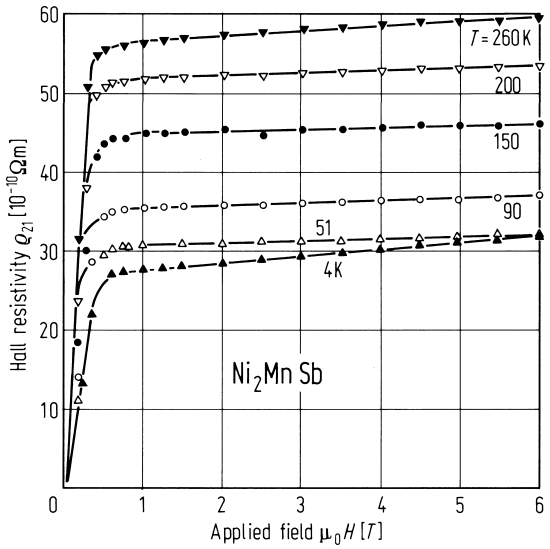

Fig. 294. Field dependence of the Hall resistivity of Ni_2MnSb at different temperatures [86H2].

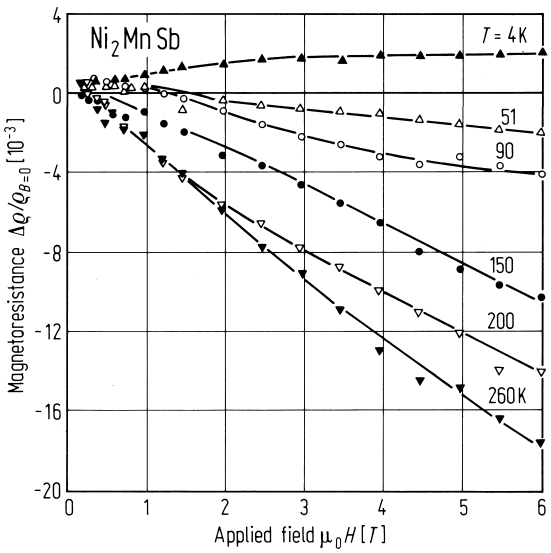

Fig. 295. Transverse magnetoresistance of Ni_2MnSb at different temperatures [86H2].

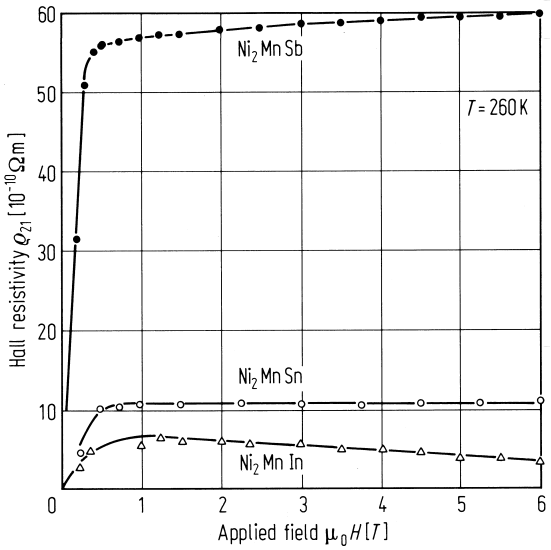

Fig. 296. A comparison of the anomalous Hall effect (AHE) in three systems Ni_2MnSb, Ni_2MnSn and Ni_2MnIn [86H2].

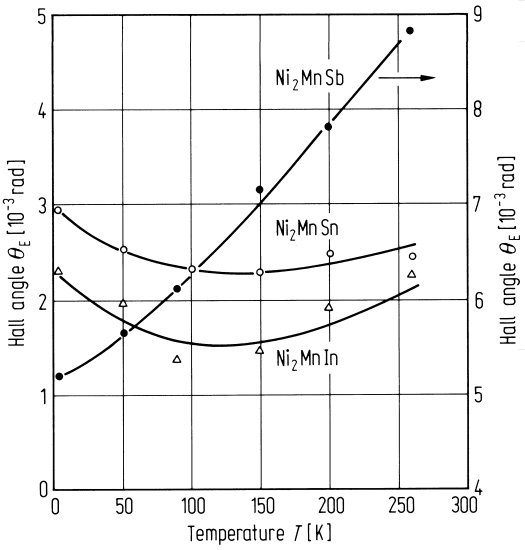

Fig. 297. Effective Hall angle plotted as a function of temperature. The plot is used to distinguish the macroscopic origins of the anomalous Hall effect (AHE) [86H2].

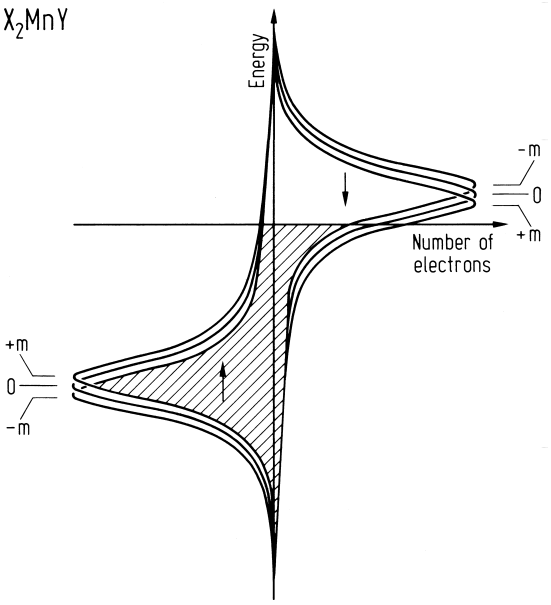

Fig. 298. Density of states for the d-level of Mn in X_2MnY. The up spin states form a common d-band with the X-atoms but the spin down electrons are excluded from the region of the 3d shell of Mn. The spin orbit coupling removes the degeneracy of the m substates in an external magnetic field [86H2].

Summary

Conclusions concerning galvanometric effects derived from the density of states (Fig. 298) are:

- The AHE arises from the down-spin electrons in the hybridised d-orbitals of the X- and Mn atoms.
- The negative magnetoresistance arises from the inelastic transfer between up and down spin states in the hybridised d orbitals of the X- and Mn-atoms.
- The ordinary Hall effect reflects the competitive effects that up and down spin Mn-d states have on states at the Fermi energy.

Assuming a rigid band model, and that the Fermi surface is fixed throughout the series In→Sn→Sb, then the calculations for Ni_2MnSn [80I1] can be used to predict the tendency of the effective mass across the series. See Fig. 299 [86H2].

Table 61. A summary of some properties of Ni_2MnZ compounds with Z = In, Sn or Sb where p_s is the saturation moment per Mn ion at 4.2 K, T_C is the Curie temperature, R_o is the ordinary Hall coefficient and n is the number density of the carriers [86H2]. e: electrons, h: holes.

Alloy	ρ (4.2 K) [Ω m]	p_s [μ_B]	T_C [K]	a [Å]	R_o [m^3/As]	n [m^{-3}]
Ni_2MnIn	$5.98 \cdot 10^{-8}$	4.57 ± 0.04	314 ± 1	6.90 ± 0.01	$-3.67 \cdot 10^{-12}$	(e) $1.7 \cdot 10^{30}$
Ni_2MnSn	$1.10 \cdot 10^{-7}$	3.88 ± 0.04	346 ± 2	6.05 [a])	$2.40 \cdot 10^{-11}$	(h) $2.6 \cdot 10^{29}$
Ni_2MnSb	$6.83 \cdot 10^{-7}$	3.70 ± 0.04	360 [a])	6.01 ± 0.01	$7.84 \cdot 10^{-11}$	(h) $8.0 \cdot 10^{28}$

[a]) Literature value; not measured in this work.

X = 1B: Ag
Y = 4A: Gd, Tb, Dy
Z = 3B: In

The ordinary Hall coefficient R_0 is positive for all compounds, whereas the spontaneous Hall coefficient R_s is negative for the Gd compounds. The magnitude of R_s increases with x for $x \leq 0.1$. The results were interpreted using a localised spin model.

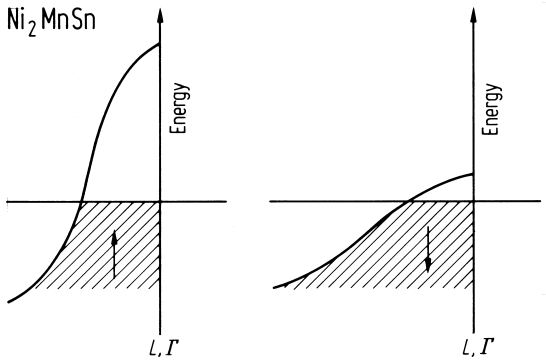

Fig. 299. Shape of the majority and minority spin energy bands in the vicinity of the L and Γ points of Ni_2MnSn [86H2].

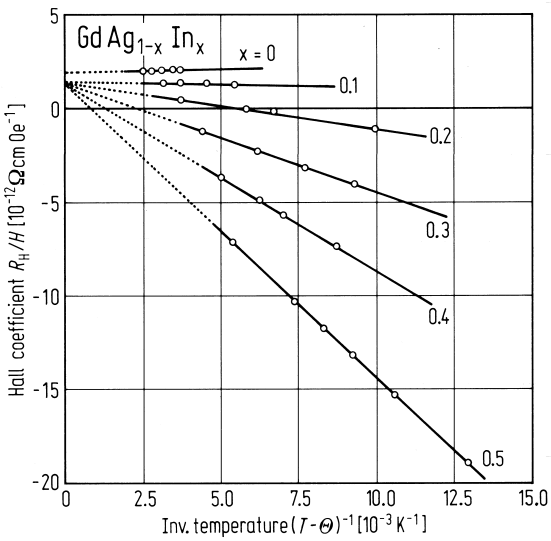

Fig. 300. Effective Hall coefficient R_H/H as a function of $(T-\Theta)^{-1}$ for $GdAg_{1-x}In_x$ compounds [80Y1].

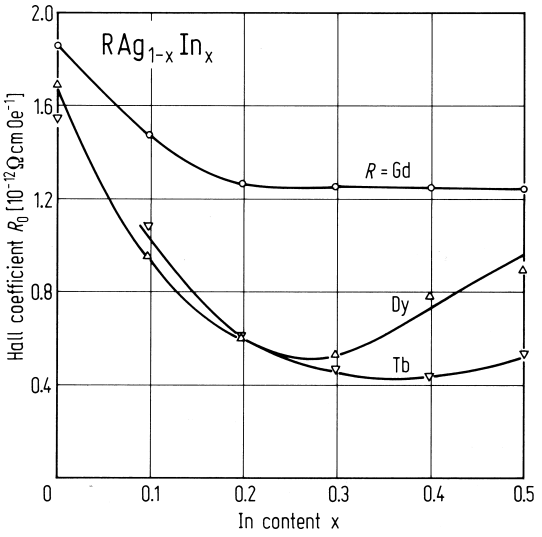

Fig. 301. A plot of the ordinary Hall coefficient R_o against x for $RAg_{1-x}In_x$ compounds with R = Gd, Dy, Tb [80Y1].

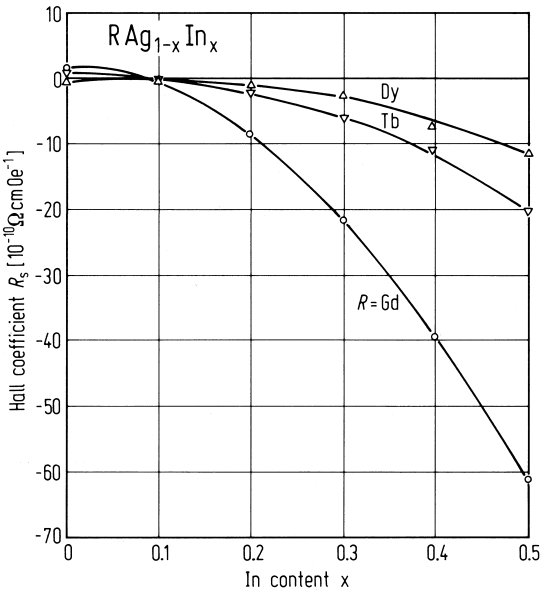

Fig. 302. A plot of the spontaneous Hall coefficient R_s against x for $RAg_{1-x}In_x$ compounds with R = Gd, Dy, Tb [80Y1].

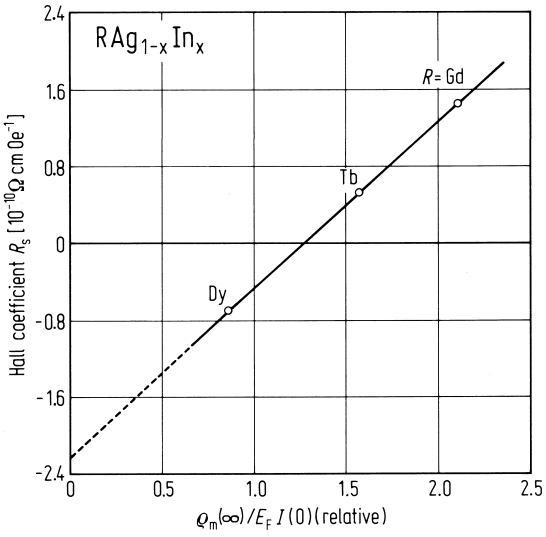

Fig. 303. A plot of the spontaneous Hall coefficient R_s against $\rho_m(\infty)/E_F I(0)$ for $RAg_{1-x}In_x$ compounds with R = Gd, Dy, Tb [80Y1]. $\rho_m(\infty)$: spin disorder resistivity, $I(0)$: magnetic moment at 0 K.

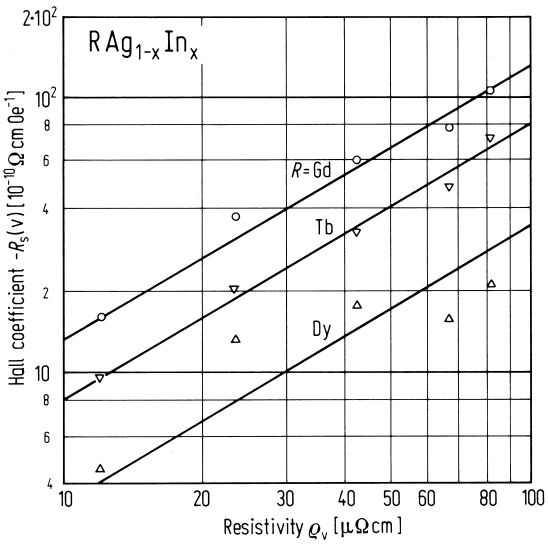

Fig. 304. A plot of the Hall coefficient $R_s(v)$ vs. ρ_V for $RAg_{1-x}In_x$ compounds with R = Gd, Dy, Tb [80Y1].

X = 1B: Cu
Y = 4A: Ce
Z = 3B: In

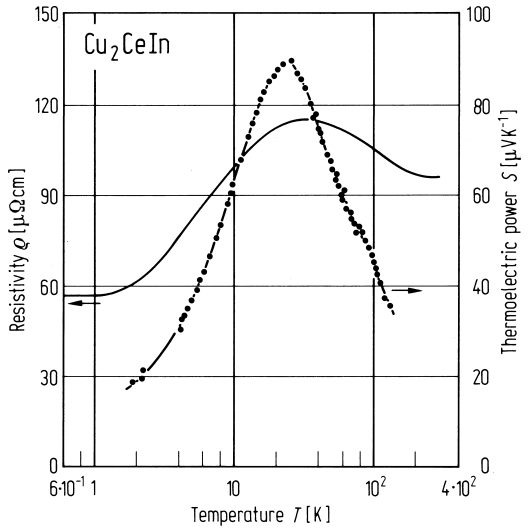

Fig. 305. Electrical resistivity and thermoelectric power in Cu_2CeIn [88T3].

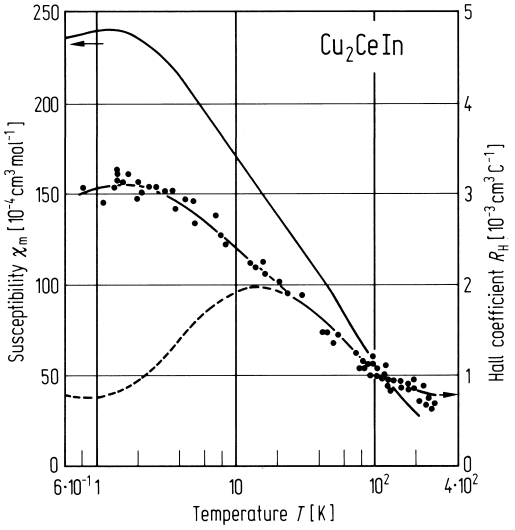

Fig. 306. Magnetic susceptibility and Hall coefficient in Cu_2CeIn [88T3]. Dashed curve: theoretical Hall effect.

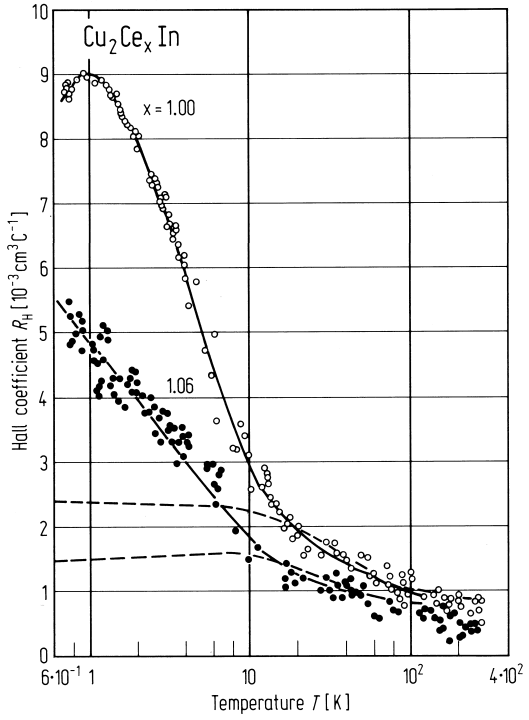

Fig. 307. Temperature dependence of the Hall coefficient for a Cu_2CeIn single crystal and $Cu_2Ce_{1.06}In$ polycrystal. The broken curves are calculated based on skew scattering [87O2].

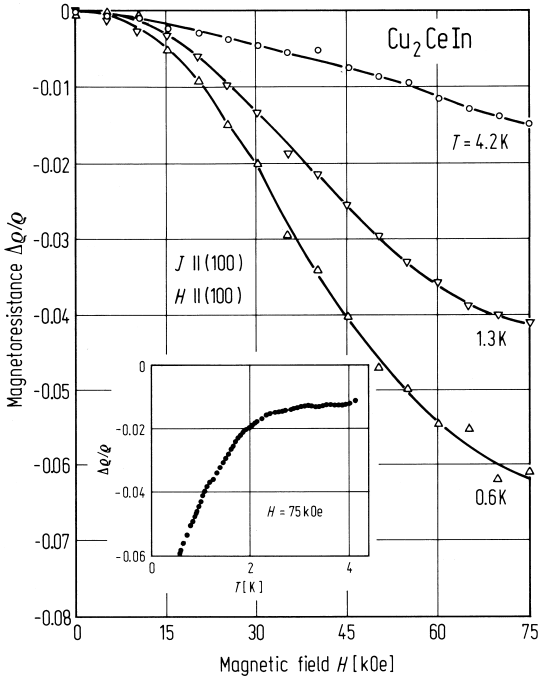

Fig. 308. Field dependence of the transverse magnetoresistance for a Cu_2CeIn single crystal. The inset shows the temperature dependence of magnetoresistance under 75 kOe [87O2].

$C1_b$ XYZ

X = 8A: Co, Ni, Pt; 1B: Cu, Au
Y = 7A: Mn
Z = 4B: Sn; 5B: Sb

Interest in $C1_b$ compounds, particularly NiMnSb, arose from band structure calculations [83G1] predicting them to be half-metallic ferromagnets. A schematic band structure is shown in Fig. 309 from which it may be seen that the minority spin band has a gap at the Fermi level, whereas the majority spin band is cut by the Fermi level. As a consequence, there is complete spin polarisation of the conduction electrons at the Fermi level.

Analysis of the Hall effect measurements indicates a strong exchange coupling between local magnetic moments and conduction electrons (holes). Consequently, the local spin polarisation persists to temperatures well above the Curie temperature.

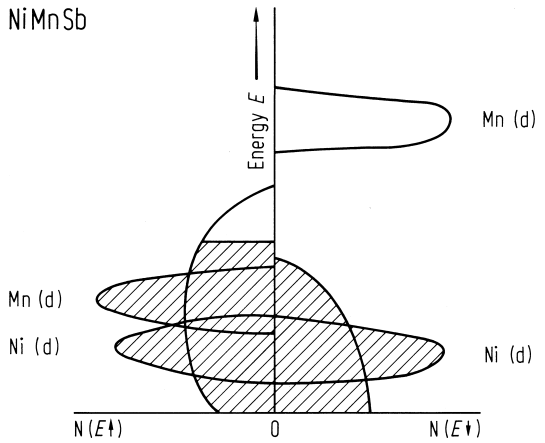

Fig. 309. Schematic diagram of the energy bands in NiMnSb [87O3].

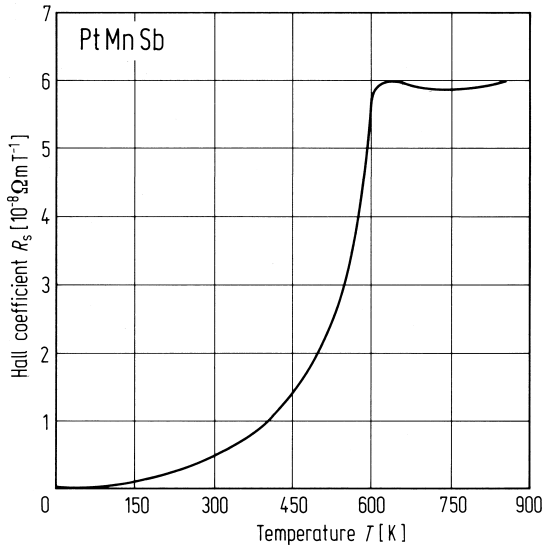

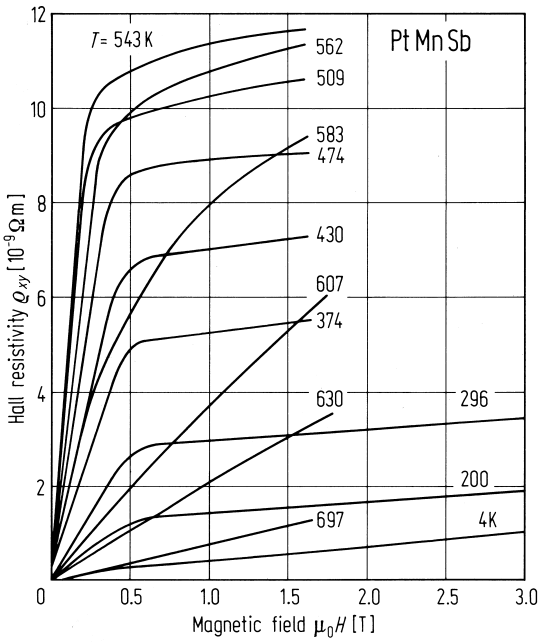

Fig. 310. Hall resistivity ρ_{xy} of PtMnSb at different temperatures [87O3].

Fig. 311. Coefficient R_s of the anomalous Hall effect plotted as a function of temperature for PtMnSb [87O3].

Table 62. Skew scattering (ϕ) and side jump (ΔL) contributions to the anomalous Hall effect [87O3].

	ϕ	ΔL [Å]
NiMnSb	– 0.037°	0.48
PtMnSb	– 0.017°	0.43
AuMnSb	– 0.76°	0.56
CoMnSb	1.1°	0.08
PtMnSn	1.2°	0.14

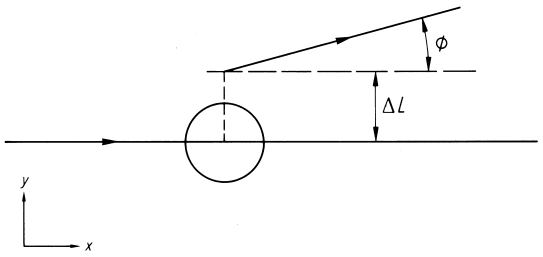

Fig. 312. Asymmetric scattering of charge carriers with spin up, due to skew scattering ϕ and side jump ΔL. For an electron with spin down $\phi \rightarrow -\phi$ and $\Delta L \rightarrow -\Delta L$. The spin up and down directions refer to the *z* axis [87O3].

1.5.5.6.3 Superconductivity

Superconductivity in Heusler alloys has primarily focused on compounds containing lanthanide elements. However, there have been some limited reports on transition metal compounds.

X_2YZ X = 3d, Y = 4d

X = 8A: Ni
Y = 5A: Nb
Z = 3B: Al, Ga; 4B: Sn

Ni_2NbZ

Critical temperatures up to 2.9 K were reported for compounds in this series which have been classified as intermediate coupled systems.

Interest in Heusler alloys containing rare earth elements arose from the possibility of the co-existence of long-range magnetic order and superconductivity [85J3]. The fact that they readily form a single phase $L2_1$ structure also made them attractive. It is thought that the co-existence of superconductivity and magnetic order arises from the relative weakness of the exchange spin flip (pair breaking) interaction between the closed 4f shells of the magnetic atoms and the conduction electrons. A possible source of complication is the degree of atomic order which is often not specified but is known to affect the magnetic properties.